WAVELENGTH AVERAGE VELOCITY ESTIMATOR FOR ULTRASOUND ELASTOGRAPHY

Eduardo A. Gonzalez[1], Juvenal Ormachea[2], Kevin J. Parker[2] and Benjamín Castaneda[1]
[1]Laboratorio de Imágenes Médicas, Pontificia Universidad Católica del Perú, Lima, Perú
[2]Department of Electrical and Computer Engineering, University of Rochester, New York, USA

ABSTRACT

A number of shear wave speed estimators have been developed for crawling wave sonoelastography. In this study, a new low-cost estimator based on spatial wavelength averaging along the slow-time domain is presented while assessing its performance through gelatin-based inclusion and homogeneous phantoms. Results showed favorable estimation mean accuracy (93.8%) on the homogeneous phantoms at different concentrations. However, underestimation is present in stiffer inclusions with size smaller than the true wavelength of the interference pattern (83.4% mean accuracy). Still, the new approach's differentiation of stiffness allows rapid visualization of a tissue as a qualitative imaging technique. Moreover, the estimator results are suitable for further processing as a reference mask implemented in several shear wave speed estimators.

Index Terms— elastography, crawling waves, shear waves

1. INTRODUCTION

Elastography methods enable radiologists to detect and localize stiffness variation by exciting the tissue, analyzing its response behavior and displaying the response in an elasticity map, where increased stiffness is differentiated from an examined region of interest (ROI) [1]. Among the techniques, crawling wave sonoelastography (CWS) provides quantitative information regarding the Young's modulus with the application of two opposing mechanical vibration sources that generate a moving interference pattern or crawling waves (CrW). Doppler image frames of the CrWs have sufficient information to measure the local spatial frequency through a shear wave speed (SWS) estimator [2].

CWS feasibility and performance has been validated in several *ex vivo* experiments. For instance, Castaneda *et al*. [3] reported stiffness differentiation between cancerous and normal tissue in prostate with 80% accuracy. Likewise, Hoyt *et al*. [4] generated 3-D reconstruction of porcine liver with consistent boundaries of a radiofrequency ablation lesion. Additionally, CWS has proven the capability to differentiate shear modulus between relaxed and contracted human skeletal muscle, making it feasible for *in vivo* characterization [5].

In elasticity techniques with mechanical and acoustic radiation force excitation, the estimation of SWS is usually derived from time to peak (TTP) displacement analysis, wavefront tracking or local frequency estimators (LFE) [6]. Regarding the estimators for CWS, Wu *et al*. [2] applied a LFE based on filter banks to assess CrW spatial frequency while Zhang *et al.* [7] calculated it with an implemented semi-automatic interface based on pattern recognition. Similarly, other estimators focus on phase derivation measurements along slow time (i.e. over a number of acquired frames) [8] and lateral dimension [9] to compute 1-D velocity maps. Furthermore, Hoyt *et al.* proposed a real-time 2-D estimator based on autocorrelation techniques [5]. Recently, Rojas *et al*. [10] introduced an estimator based on dominant component analysis of AM-FM demodulation.

Despite the numerous SWS methods currently described in literature, the presence of artifacts is still reported in most of the reconstructed elasticity images. Therefore, a more robust algorithm for SWS estimation is constantly being researched, and serves as the motivation for the present study. Here, a new SWS estimator based on CWS is presented. Feasibility and performance of the proposed method were demonstrated in tissue mimicking phantoms representing homogeneous and heterogeneous tissues. Additionally, preliminary results were compared with the phase derivative approach [10] in inclusion experiments.

2. THEORY

The proposed method, named the Wavelength Average Velocity Estimator (WAVE), is based on the conventional crawling wave's propagation proposed by Wu *et al*. [2].

A. Crawling Wave Sonoelastography

Two external low-frequency vibration sources are placed at the lateral sides of a tissue, achieving a vertical interference moving pattern described by:

$$|u(x,t)|^2 = 2e^{-\alpha_c D}[\cos(2k + \Delta k)\, x + \Delta\omega t] \qquad (1)$$

where D is the distance between the sources, α_c the attenuation of the medium, k the wave number, ω the

vibration frequency and $\Delta\omega$ the offset frequency between the sources. An ultrasound probe placed at the top of the tissue acquire color radiofrequency (CRF) data over a number of frames. Then, a sonoelasticity video is generated using Miller's spectral moment estimator [11] on the acquired in-phase quadrature signals, as shown in Fig. 1. The estimated variance is normalized along the lateral and temporal axis to in order to reduce the noise level.

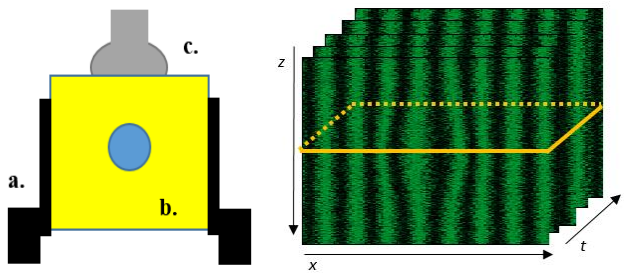

Fig. 1. Left side: Conventional crawling wave setup. (a) Vibration source, (b) examined tissue, (c) probe. Right: sonoelasticity video showing the interference pattern produced by the vibration sources. WAVE is computed over each depth slice across the lateral and temporal dimension to generate an SWS image.

B. *Wavelength Average Velocity Estimator*

The proposed estimator provides a resulting lateral vector of local SWS values by analyzing the displacement of the interference pattern in a lateral profile. Therefore, WAVE is computed over each slice across the lateral and temporal dimension in order to generate a complete SWS image. At the pre-processing stage, a moving filter is implemented on each slide of depth (see Fig. 1) for SNR enhancement and suppression of reflection artifacts, following the framework of Castaneda *et al.* [3]. The filter is designed as a 2D band-pass centered at the normalized temporal frequency f_t and local frequency range f_k. The first parameter depends on the frequency offset Δf and frame rate (FR), while the second is set according to the desired elasticity limits e_{high} and e_{low}:

$$f_t = \Delta f / FR \tag{5}$$

$$f_k \propto [e_{high} \;\; e_{low}] \tag{6}$$

Given a lateral profile of the interference pattern, shear wave speed c_s is defined as:

$$c_s = \lambda f, \tag{7}$$

where f is the vibration frequency induced into the tissue and λ is two times the lateral distance between peaks of the interference pattern, which is assumed to be parallel to the axial axis. Considering that $\lambda/2$ is narrow enough to be included in a homogenous tissue, a partial SWS vector containing the average velocity between peaks is generated for each frame of the sonoelasticity video, as shown in Fig. 2. Boundary regions with no detected peaks in-between are filled with extrapolated c_s of the partial SWS vector. Then, the resulting local SWS vector is calculated as the average of the partial SWS vectors along the temporal dimension. The same process is repeated for each slice until a complete SWS image is depicted. Finally, a second SWS image obtained from valley recognition is computed as well for further average it with the first one, enhancing smoothness.

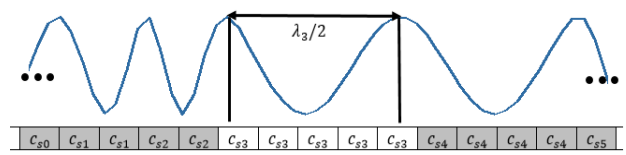

Fig. 2. Interference pattern along the lateral dimension at a selected depth and frame, and its estimated partial SWS vector. The distance between peaks represent half the wavelength of the average SWS.

3. EXPERIMENTS AND RESULTS

A. *Phantom Generation and Setup*

Experiments were conducted on gelatin-based homogenous and inclusion phantoms following the procedure described by Hah *et al* [9]. Three 13 x 13 x 8 cm homogeneous phantoms were generated with 10%, 13% and 16% concentration of gelatin (300 Bloom Pork Gelatin, Gelatin Innovations Inc.), 1.8 l of degassed water, 16.2 g of Na-Cl, 36 g of graphite (Graphite Powder, Fisher Scientific Inc.), and 2.7 g of agar (Technical Grade Agar, Fisher Scientific Inc.). Likewise, a 10mm-diameter cylinder inclusion with 10% gelatin concentration is added at 26 mm depth and 19mm width (centered along the lateral dimension) of the background phantom with 8% concentration. Finally, ground truth values were estimated with mechanical measurements (MM) applied in all gelatin concentration phantom, following the procedure described by Ormachea *et al.* [12]. The Kelvin Voigt Fractional Derivative (KVFD) model was implemented for fitting each of the acquired stress-relaxation curves. Measured SWS of the 10%, 13% and 16% gelatin phantoms were approximately 4 m/s, 5 m/s and 6 m/s, respectively, as shown in the results section.

For all the experiments, sonoelasticity data acquisition was conducted using the same CrW setup. Two mechanical mini-shakers (4810 Brüel & Kjaer, Naerum, Denmark) were placed at opposite lateral sides of the inclusion phantom, vibrating from 160 to 500 Hz in 20 Hz steps. The excitation signals, differentiated by 0.4 Hz, were generated with a dual channel function generator (AFG3022B, Tektronix, Beaverton, OR, USA) and an amplifier (5530, AE Techron, Elkhart, IN, USA). CRF data was acquired using a linear transducer M12L (GE Healthcare, Wauwatosa, WI, USA) connected to a GE LOGIQ 9 ultrasound system (GE Healthcare, Wauwatosa, WI, USA). Regarding the moving filter configuration, the desired elasticity range was set from 1 m/s to 7 m/s. Finally, a 60 x 38.4 mm windows size was used for the CRF data acquisition and analysis.

B. Results

The resulting mean and standard deviation of SWS values for each homogeneous phantom are depicted in Fig. 3. Estimation was conducted over a small windows of 15mm width and 30 mm depth located at the center of the ROI. Despite the slight underestimation from the MM present throughout all concentrations and frequencies (mean SWS of 3.84 m/s, 4.89 m/s and 5.76 m/s for 10%, 13% and 16% gelatin concentration, respectively), WAVE results closely followed the ideal homogenous shear wave speed. However, a decrease of accuracy is observed in frequencies below 200 Hz and in nearly all of the 16% gelatin frequencies. This is understandable since imaging stiffer tissues using low excitation frequencies would produce fewer interference patterns in a single frame, detecting one or two pairs of peaks at most. Hence, the resolution of the partial SWS vectors is compromised and estimation errors are induced. In contrast, the standard deviation (STD) remained constant through the frequency range (0.053 m/s, 0.105 m/s and 0.132 m/s for 10%, 13% and 16% gelatin concentration, respectively).

SWS plots for the heterogeneous phantom are shown in Fig. 4. Here, two square windows of 8 mm were used to quantify mean SWS and STD (see Fig.5). Similar to homogeneous assessments, crawling waves with vibration frequencies below 200 Hz adversely affected the estimator's accuracy for both inclusion (3.43 ± 0.02 m/s) and background regions (3.29 ± 0.11 m/s). Subsequently, comparable accuracy with the homogeneous evaluation is observed in the inclusion region just above 360 Hz (3.86 ± 0.067 m/s).

Fig. 5 depicts the generated SWS images of the inclusion phantom at a low (280 Hz) and high frequency (500 Hz). Additionally, SWS images obtained from the phase derivative (PD) estimator proposed by Hah *et al.* [9] are presented for quality comparison. A smoothing filter with kernel size of 20% in the lateral dimension is used for jitter suppression in phase estimation. Fig. 4a and Fig. 4c reflects the results in Fig. 3, while Fig. 4b and Fig. 4d provide better boundary definition and SWS accuracy at the cost of increased artifacts.

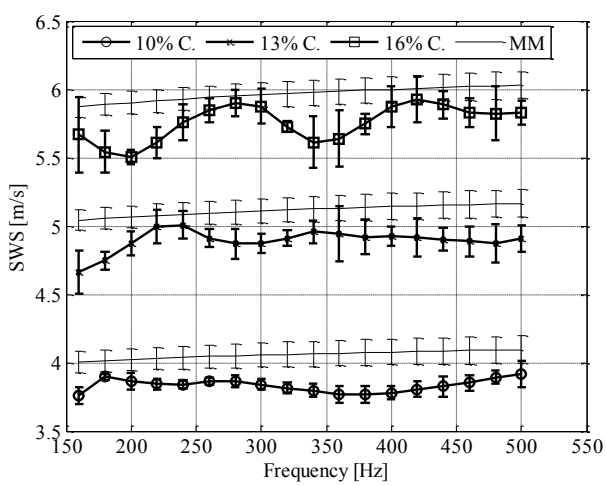

Fig. 3. SWS estimation obtained from WAVE method in homogenous phantom of 10%, 13%, and 16% gelatin concentration with their respective mechanical measurements.

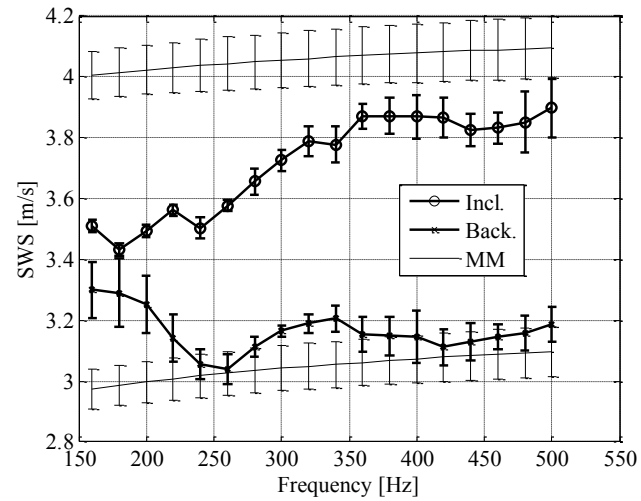

Fig. 4. SWS estimation (m/s) of a heterogeneous phantom of 10% and 8% for inclusion and background region with their respective mechanical measurements.

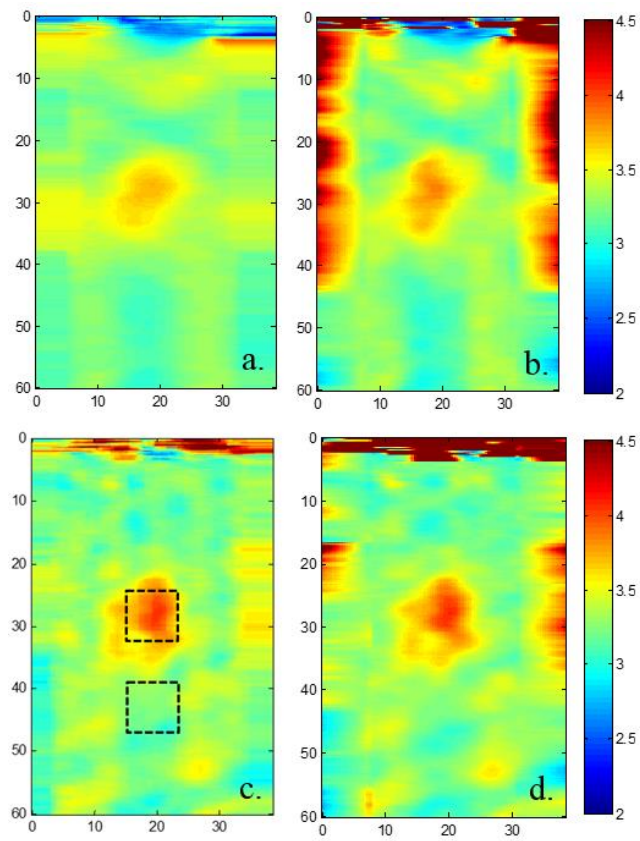

Fig. 5. SWS images (m/s) of an inclusion phantom at (a, b) 280 Hz and (c, d) 500 Hz vibration frequency. Left side: WAVE. Right side: PD. Measurement are shown in mm. Squares windows of 8mm were used for mean and STD estimation.

4. DISCUSSION

WAVE results suggest favorable SWS estimation on homogenous phantoms (93.78% accuracy) with the exception of 16% concentration and frequencies below 200 Hz due to the low number of peaks along the lateral profile, as noted in the results section. In practice, limitations of the algorithm application may be found on stiffer lesions or regions where the typical excitation frequency is set under 200 Hz (i.e. prostate and ablated liver).

Likewise, a considerable underestimation of the inclusion in the heterogeneous phantom experiment was observed. For frequencies below 350 Hz, the measured distance between the interference pattern's peaks were wider than the inclusion diameter. Thus, a complete interference pattern inside the inclusion was undetected, resulting in weighted average estimations of SWS between the inclusion and background regions. Therefore, a dependency of lesion size, stiffness and vibration frequency is introduced in the WAVE's performance.

One of the advantages of the WAVE method in comparison with the PD method is the reduction of artifacts in the boundaries of the ROI. While artifacts in the lateral sides were severely diminished mostly as a result of the wavelength extrapolation, top regions were improved as well. In practice, artifacts with high values of shear wave speed might mislead the technician into surmising that stiffer masses are present. Thus, the accuracy of diagnosis is undermined due to false-positive lesions, which are suppressed by the WAVE method.

Finally, despite the underestimation at lower frequencies, WAVE successfully differentiated between a stiffer and softer mask similar to the PD estimator, as shown in Fig. 4. Therefore, it is suitable for quick and preliminary visualization of a tissue as a qualitative imaging technique, which might benefit image-guided surgery procedures. Furthermore, it could be used as a reference mask for additional SWS estimators in order to compensate for estimation errors due to low vibration frequencies and high stiffness inclusions, as well as enhance the estimation accuracy on inclusion boundaries.

5. CONCLUSION

In this study, a new shear wave speed estimator is proposed for ultrasound elastography based on a conventional crawling wave setup. The estimator showed favorable estimation accuracy (93.8%) on homogeneous phantoms at different gelatin concentrations. Additionally, preliminary results on inclusion phantoms demonstrate comparable performance with other approaches, such as the phase derivative estimator. However, the accuracy dependence on excitation frequency range and lesion size severely compromise its implementation as a quantitative elastography technique. Still, WAVE's differentiation in stiffness allows quick and preliminary visualization of a tissue as a qualitative imaging technique. Moreover, the estimator results are suitable for further processing as a reference mask implemented in several shear wave estimators. Simulation and experiments regarding this last observation will be conducted in future works.

6. ACKNOWLEDGEMENTS

This work was supported by the project 205-FinCYT-IA-2013 and DGI-2015-1-077, funded by the Peruvian government. The authors are grateful to Dr. Roberto J. Lavarello for his advice and guidance.

7. REFERENCES

[1] L. Gao, K. J. Parker. "Imaging of the elastic properties of tissue – A review" *Ultrasound Med. & Biol.,* vol. 22, no. 8, pp. 959-977, 1996.

[2] Z. Wu, L. S. Taylor, D. J. Rubens, and K. J. Parker, "Sonoelastographic imaging of interference patterns for estimation of the shear velocity distribution in biomaterials," *J. Acoust. Soc. Am.,* vol. 120, no. 1, p. 535-545, 2006.

[3] B. Castaneda, L. An, S. Wu, L. Baxter, J. Yao, J. Joseph, K. Hoyt, J. Strang, D. Rubens and K. J. Parker. "Prostate Cancer Detection Using Crawling Wave Sonoelastography". *Proc. SPIE, Medical Imaging 2009: Ultrasonic Imaging and Signal Processing*, vol. 7265, no. 13.

[4] K. Hoyt, B. Castaneda, and K. J. Parker, "Two-dimensional sonoelastographic shear velocity imaging," *Ultrasound Med. & Biol.*, vol. 34, no. 2, pp. 276–288, 2008.

[5] K. Hoyt, B. Castaneda, and K. J. Parker, "Muscle tissue characterization using quantitative sonoelastography: Preliminary results," *Ultrasonics Symposium*, IEEE, pp. 365–368, 2007.

[6] S. Rosenzweig, M. Palmeri, N. Rouze, S. Lipman, E. Kulbacki, J. Madden J, T. Polascik and K. Nightingale. "Comparison of concurrently acquired in vivo 3D ARFI and SWEI images of the prostate". *Ultrasonics Symposium*, IEEE. pp. 97-100, 2012.

[7] M. Zhang, B. Castaneda, Z. Wu, P. Nigwekar, J. V. Joseph, D. J. Rubens and K. J. Parker. "Congruence of imaging estimators and mechanical measurements of viscoelastic properties of soft tissues". *Ultrasound in Med. & Biol*., vol. 33, no. 10, pp. 1617-1631, 2007.

[8] K. Lin, J. McLaughlin, D. Renzi and A. Thomas. "Shear wave speed recovery in sonoelastography using crawling wave data" *J. Acoust. Soc. Am.*, vol. 128, no. 1, pp. 88-97, 2010

[9] Z. Hah, C. Hazard, B. Mills, C. Barry, D. Rubens, K. J. Parker. "Integration of crawling waves in an ultrasound imaging system: Part 2. Signal processing and applications". *Ultrasound Med Biol.*, vol. 38, pp. 312–323, 2012

[10] R. Rojas, J. Ormachea, A. Salo, P. Rodriguez, A. Lerner, and B. Castaneda, "Crawling waves speed estimation based on dominant component analysis amfm demodulation." in *International Tissue Elasticity Conference (ITEC)*, p. 100, 2013.

[11] K. Miller, M. Rochwarger. "A Covariance Approach to Spectral Moment Estimation". *IEEE Transactions on Information Theory*, vol. 18, no. 5, 1972.

[12] J. Ormachea, R. Rojas, P. Rodriguez, R. Lavarello, K. J. Parker and B. Castaneda. "Shear Wave Speed Estimation from Crawling Wave Sonoelastography: A comparison between AM-FM Dominant Component Analysis and Phase Derivation Methods". *IEEE International Ultrasonic Symposium*, pp. 2327-2330, 2014